Multiple-Beam Interference-Enabled Broadband Metamaterial Wave Plates

Junhao Li,[1] Huijie Guo,[2] Tao Xu,[3] Lin Chen,[1,*] Zhihong Hang,[3] Lei Zhou,[2] and Shuqi Chen[4]

[1]*Wuhan National Laboratory for Optoelectronics, Huazhong University of Science and Technology, Wuhan 430074, China*
[2]*State Key Laboratory of Surface Physics and Key Laboratory of Micro and Nano Photonic Structures (Ministry of Education), Fudan University, Shanghai 200433, China*
[3]*College of Physics, Optoelectronics and Energy and Collaborative Innovation Center of Suzhou Nano Science and Technology, Soochow University, Suzhou 215006, China*
[4]*Laboratory of Weak Light Nonlinear Photonics Ministry of Education School of Physics, Teda Applied Physics Institute, Nankai University, Tianjin 300071, China*

Metamaterials have generated considerable research interest in manipulating light polarization states, but many proposals suffer from the issue of narrow bandwidth and/or low transmission efficiency. We show that a classical multiple-beam interference mechanism can be employed to modulate the phase dispersion of transmitted waves in metamaterials, which motivates us to establish a general strategy to achieve a constant cross-polarization phase difference by independently controlling the phase dispersion for the two orthogonal polarizations. We derive a criterion under which the cross-polarization phase difference across the metamaterial devices can be maintained at a nearly constant value over a wide frequency band. The codesigned metamaterial quarter-wave plate presents an excellent polarization conversion performance over a broad frequency band. We also employ full-wave simulations to demonstrate a broadband quarter-wave plate at telecom and terahertz frequencies based on the proposed design strategy. Our findings can stimulate making high-performance broadband optical devices based on various metamaterials in different frequency domains, and impact numerous photonic applications.

I. INTRODUCTION

Manipulating the polarization states of electromagnetic (em) waves is of great importance in fundamental physics and many free-space and integrated photonics applications. Traditionally, conversion between different types of polarization states is realized with wave plates (WPs) made by natural birefringent crystals and subwavelength gratings, but which require large device thickness to accumulate the phase difference due to the limited birefringence index (Δn, typically less than 0.3) [1,2]. Furthermore, such WPs inherently exhibit a narrow operation bandwidth because of the frequency-dependent property of the birefringent index.

Metamaterials (MTMs) have provided an unprecedented approach for the extreme control of em waves with controllable amplitude, phase, and polarization at subwavelength scales [3–10]. To date, many MTM-based WPs have been proposed and/or demonstrated over the entire spectral regime from microwave to visible frequencies. Moreover, they offer many advantages, such as compactness, flexibility, and easy integration on a chip, which are

unachievable with traditional WPs based on birefringent crystals. Although the birefringent index is larger for MTMs than birefringent crystals, many MTM-based WPs exhibit limited operation bandwidths since their building blocks are typically comprised of some resonant structures, yielding significant phase dispersion [11–16]. A general solution to enlarge the operation bandwidth of MTM WPs is to use decoupled resonance to enable a nearly constant phase difference over a wide spectral range [17–21]. However, that scheme is generally applicable to the design of reflection-mode WPs, under which one merely needs to control the dispersion of the reflection phase since the reflection amplitude is typically near 100%. Such a scheme faces significant limitation in the design of transmission-mode WPs (more useful in applications) since a constant phase difference is accompanied by frequency dependent transmission amplitude within a wide spectral range [22–28]. While promising steps have been taken to enable high-efficiency broadband WPs based on double-stacked anisotropic MTM structures [29–31], it is challenging to fabricate these structures with nonoverlapping cross sections along the propagation direction, especially when they are scaled down for optical frequencies.

---

*chen.lin@mail.hust.edu.cn

Multiple-beam interference (MBI), arising from multiple internal reflections in a film, is a fundamental phenomenon for light. Although several papers have considered the influence of the MBI effect on the optical properties of MTMs, these studies merely focused on using MBI to modulate the amplitude of transmitted or reflected beams [32,33] or explained the additional reflection phase caused by MBI [21]. We note that there is no report on using MBI to manipulate the transmission or reflection phase in MTMs. In this paper, we first propose to use the additional phase imparted by MBI to manipulate the overall transmission phase so as to achieve a nearly flat phase difference over a wide spectral range. We can thus construct broadband MTM devices, such as quarter-wave plates (QWPs), which require the constant maintenance of the phase difference of the transmitted waves over a wide spectral range. As an example, we establish a general strategy to build high-performance broadband WPs by introducing MBI to manipulate the transmission-phase dispersion for anisotropic MTMs. The cross-polarization phase difference dispersion can be cancelled out by specifically designing the geometrical parameters of the anisotropic MTMs to generate an additional positive or negative phase shift for the two orthogonal polarization directions, thanks to the contribution of constructive or destructive interference. As a proof-of-concept demonstration, an anisotropic MTM made by a metal and dielectric multilayer with a very large birefringent index is designed to enable a flat cross-polarization phase difference. We further fabricate an anisotropic MTM broadband WP and experimentally characterize its excellent circular-to-linear polarization conversion abilities over a wide frequency range (6.73–7.60 GHz). We also employ full-wave simulations to demonstrate broadband QWPs at telecom and terahertz frequencies based on the proposed design strategy. In comparison to previous works on broadband WPs made by anisotropic MTMs [29–31], the general design strategy presented in this paper does not require double-stacked MTMs of nonoverlapping cross sections along the propagation direction. Thereby, it can notably relax the fabrication difficulties over the entire spectral range. Our results, based on classical MBI to control the phase dispersion, can be used to construct broadband transmission-mode optical devices based on various metamaterials in different frequency domains, and might promote numerous photonic applications.

II. RESULTS AND DISCUSSION

A. MBI for phase modulation

The idea of phase dispersion cancellation for anisotropic MTMs described in this paper is inspired by examining the phase shifts to the reflection and transmission coefficients imparted by MBI. Let us first revisit the working

principle of a Fabry-Perot interferometer, in which MBI is used to realize sharp transmission peaks. Two prerequisites, an ultra-long optical cavity (tens of thousands of wavelengths) and highly reflective interfaces, are required to guarantee the sharp transmission peaks. However, the optical length of the system investigated in this study is comparable to the wavelength, and the reflectivity at the interface is very low in comparison to a Fabry-Perot interferometer. Consequently, it is possible to obtain a relatively broader transmission peak or dip, which, therefore, leaves us with a wide spectral band to use MBI to manipulate the phase dispersion of the transmitted waves. As shown in Fig. 1, consider a four-layer system consisting of semi-infinite air (layer one, $n_1 = 1$), a high-index film (layer two, n_2, thickness h_2), a lower-index substrate (layer three, n_3, thickness h_3), and semi-infinite air (layer four, $n_4 = 1$). Here, it is assumed that n_3 is a constant and $n_3 < n_2$. The propagation constant for each layer is expressed as $k_j = 2\pi n_j f /c$, where n_j denotes the refractive index of layer j $(= 1, 2, 3, \text{ or } 4)$, f represents the light frequency, and c is the light velocity in air. Two steps are required to retrieve the trasmission efficient, t_0. First, by treating layer two together with its left- and right-side boundaries as cavity one, the reflection and transmission coefficients shown in Figs. 1(a) and 1(b) can be deemed as the superpositions of multiple reflections and transmissions at the
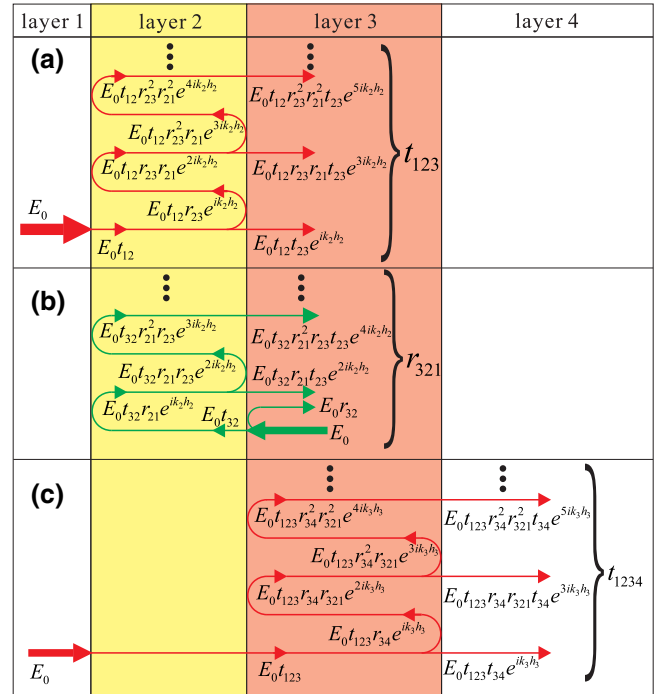

FIG. 1. The schematic of a four-layer system showing how multiple reflections and transmissions at the interfaces contribute to the transmission and reflection coefficients, (a) t_{123}, (b) r_{321}, and (c) t_0.

two interfaces

$$t_{123} = t_{12}t_{23}e^{ik_2h_2} + t_{12}r_{23}r_{21}t_{23}e^{3ik_2h_2} + t_{12}r_{23}^2r_{21}^2t_{23}e^{5ik_2h_2}$$

$$+ \ldots = \frac{t_{12}t_{23}e^{ik_2h_2}}{1 - r_{21}r_{23}e^{2ik_2h_2}}, \tag{1}$$

$$r_{321} = r_{32} + t_{32}r_{21}t_{23}e^{2ik_2h_2} + t_{32}r_{21}^2r_{23}^2e^{4ik_2h_2} + \ldots = r_{32}$$

$$+ \frac{t_{32}r_{21}t_{23}e^{2ik_2h_2}}{1 - r_{21}r_{23}e^{2ik_2h_2}}, \tag{2}$$

where t_{lq} and r_{lq} are the transmission and reflection coefficients from layer l to layer q (l, q = 1, 2, 3, or 4). The substrate (layer three), cavity one described above, and the semi-infinite air (layer four) form cavity two. Thus, the overall transmission coefficient shown in Fig. 1(c) can be given as

$$t_0 = t_{123}t_{34}e^{ik_3h_3} + t_{123}r_{34}r_{321}t_{34}e^{3ik_3h_3}$$

$$+ t_{123}r_{34}^2r_{321}^2t_{34}e^{5ik_5h_5} + \ldots = \frac{t_{123}t_{34}e^{ik_3h_3}}{1 - r_{321}r_{34}e^{2ik_3h_3}}, \tag{3}$$

where t_{34} and r_{34} follow the Fresnel Equations as $t_{34} = 2n_3/(n_3 + n_0)$ and $r_{34} = (n_3 - n_0)/(n_3 + n_0)$. By substituting Eqs. (1) and (2) into Eq. (3), and taking the argument of t_{1234}, the total transmission phase of the four-layer system can be written as

$$\arg t_0 = \arg[t_{12}t_{23}t_{34}e^{i(k_2h_2+k_3h_3)}]$$

$$+ \arg\frac{1}{1 - r_{21}r_{23}e^{2ik_2h_2}} + \arg\frac{1}{1 - r_{321}r_{34}e^{2ik_3h_3}}$$

$$= \arg t'_0 + \Delta\phi_1 + \Delta\phi_2, \tag{4}$$

where $t'_0 = t_{12}t_{23}t_{34}e^{i(k_2h_2+k_3h_3)}$ represents the transmission coefficient of light passing through the four-layer system without the involvement of phase modulation from the interface reflection, and $\Delta\phi_1$ and $\Delta\phi_2$ are the additional transmission phases caused by the MBI of cavities one and two, respectively. Throughout the paper, we use τ_ϕ to indicate the derivative of ϕ with respect to frequency. The derivative functions of $\Delta\phi_1$ and $\Delta\phi_2$ with respect to frequency, $\tau_{\Delta\phi_1}$ and $\tau_{\Delta\phi_2}$, can be expressed as (see Note 1 in the Supplemental Material for more details about the derivation process [34])

$$\tau_{\Delta\phi_1} = \frac{\sin\phi_{c1}\frac{d|r_{21}r_{23}|}{df} + |r_{21}r_{23}|(\cos\phi_{c1} - |r_{21}r_{23}|)\tau_{\phi_{c1}}}{(|r_{21}r_{23}|\sin\phi_{c1})^2 + (1 - |r_{21}r_{23}|\cos\phi_{c1})^2}, \tag{5}$$

$$\tau_{\Delta\phi_2} = \frac{|r_{34}|\sin\phi_{c2}\frac{d|r_{321}|}{df} + |r_{321}r_{34}|(\cos\phi_{c2} - |r_{321}r_{34}|)\tau_{\phi_{c2}}}{(|r_{321}r_{34}|\sin\phi_{c2})^2 + (1 - |r_{321}r_{34}|\cos\phi_{c2})^2}, \tag{6}$$

where $\phi_{c1} = 2k_2h_2 + \phi_{r_{21}} + \phi_{r_{23}}$ and $\phi_{c2} = 2k_3h_3 + \phi_{r_{321}}$ determine the interference condition for cavities one and two, respectively. The influences of n_2 and h_2 on ϕ_{c1}, $|t_{123}|$, and $\tau_{\Delta\phi_1}$ are investigated, as shown in Figs. 2(a)–2(c). It can be clearly seen that $|t_{123}|$ and $\tau_{\Delta\phi_1}$ reach the maximum (minimum) values when a constructive (destructive) interference condition $\phi_{c1} = 2m\pi$ [$\phi_{c1} = (2m + 1)\pi$] (m is an integer) is satisfied for cavity one. A higher h_2 (or larger n_2) tends to increase the maximum value of $\tau_{\Delta\phi_1}$, but shorten the monotone intervals [Fig. 2(c)]. The quantitative relationship between $|t_{123}|$, $\tau_{\Delta\phi_1}$, and n_2 is described by Eqs. (1) and (5), respectively, where $|r_{21}r_{23}|$ is monotonously increased with n_2.
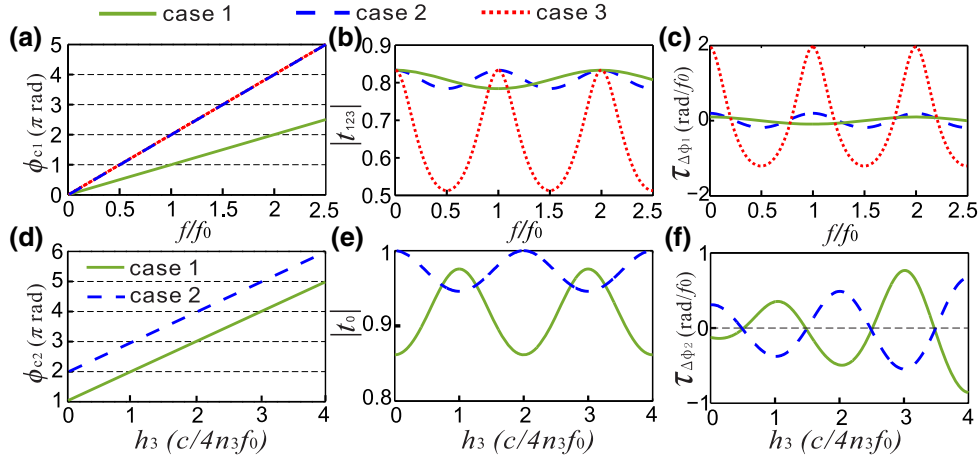

FIG. 2.   (a) ϕ_{c1}, (b) $|t_{123}|$, and (c) $\tau_{\Delta\phi_1}$ vs f with a four-layer system for the three cases. For all the three cases, the refractive indices of layers one and three remain unchanged: $n_1 = 1$ and $n_3 = 1.4$. Layer two has a varied refractive index and thickness for three different cases: $n_2 = 1.75$ and $h_2 = c/7f_0$ for case one (the green line); $n_2 = 1.75$ and $h_2 = 2c/7f_0$ for case two (the blue line); and $n_2 = 3.5$ and $h_2 = c/7f_0$ for case three (the red line). (d) ϕ_{c2}, (e) $|t_0|$, and (f) $\tau_{\Delta\phi_2}$ as a function of h_3 at the frequency of f_0. The green solid line and the blue dashed line are obtained when cavity one is under constructive and destructive interferences at f_0, associated with case one and two in Figs. 2(a)–2(c), respectively.

Moreover, it is found that the transmission phase dispersion can be significantly modulated by controlling the interference condition for cavity two, once cavity one is under a constructive or destructive interference condition as mentioned above. By incorporating the interference condition for cavity one into Eq. (2), it is possible to obtain $\phi_{r_{321}} = 0$ with $\phi_{c1} = 2m\pi$, and $\phi_{r_{321}} = \pi$ with $\phi_{c1} = (2m + 1)\pi$. Here, both $k_3 h_3$ and $\phi_{r_{321}}$ contribute to the interference condition for cavity two ($\phi_{c2} = 2k_3 h_3 + \phi_{r_{321}}$). Figures 2(d)–2(f) present the dependence of ϕ_{c2}, $|t_0|$, and $\tau_{\Delta\phi_2}$ on h_3 at $f = f_0$, in which cavity one is under the destructive interference condition for case one and the constructive interference condition for case two. Analogous to cavity one, Fig. 2(f) illustrates that $\tau_{\Delta\phi_2}$ reaches the maximum (minimum) values when the constructive (destructive) interference condition is satisfied for cavity two, namely, $\phi_{c2} = 2M\pi$ [$\phi_{c2} = (2M + 1)\pi$], where M is an integer. To briefly conclude, cavities one and two can be independently designed to modulate the transmission phase for the four-layer system.

B. Dispersionless anisotropic medium by MBI

The cross-polarization phase difference that can be introduced as layer two is anisotropic (n_2^x, n_2^y are its effective refractive indices along the x and y directions, respectively), so that the resultant four-layer system shows a distinct em response for the x and y polarizations. The total transmission coefficients for the x and y polarizations are denoted as t_0^x and t_0^y, respectively. The cross-polarization phase difference for the four-layer system can be expressed as

$$\phi_{\rm PD} = \arg t_0^y - \arg t_0^x = \phi_{\rm PD}' + \Delta\phi_1^y + \Delta\phi_2^y - \Delta\phi_1^x - \Delta\phi_2^x, \tag{7}$$

and its derived function with respect to frequency is written as

$$\tau_{\phi_{\rm PD}} = \tau_{\phi'_{\rm PD}} + \tau_{\Delta\phi_1^y} + \tau_{\Delta\phi_2^y} - \tau_{\Delta\phi_1^x} - \tau_{\Delta\phi_2^x}, \tag{8}$$

where $\phi'_{\rm PD} = \arg t_0'^y - \arg t_0'^x = 2\pi(n_2^y - n_2^x)h_2 f / c$ is the cross-polarization phase difference without the involvement of MBI. Under the assumption that $n_2^y > n_2^x$, $\tau_{\phi'_{\rm PD}}$ is positive and increases monotonously with f. To enable the dispersionless cross-polarization phase difference around a certain frequency of f_0, $\tau_{\phi_{\rm PD}}$ should be zero, that is, $\tau_{\phi'_{\rm PD}} + \tau_{\Delta\phi_1^y} + \tau_{\Delta\phi_2^y} - \tau_{\Delta\phi_1^x} - \tau_{\Delta\phi_2^x} = 0$. Here, "dispersionless" refers to the constant cross-polarization phase difference within a broad spectral band. The proper selection of n_2^y, n_2^x, and h_2 enables cavity one to interfere constructively and destructively along the x and y directions at a certain frequency of f_0, respectively. This results in $\phi'_{\rm PD} = 4\pi(n_2^y - n_2^x)h_2 f_0 / c = \pi/2$, $\tau_{\Delta\phi_1^x} = 2\pi n_2^x h_2 |r_{21}^x r_{23}^x| / [(1 - |r_{21}^x r_{23}^x|)c] > 0$, and $\tau_{\Delta\phi_1^y} =$

$-2\pi n_2^y h_2 |r_{21}^y r_{23}^y| / [(1 + |r_{21}^y r_{23}^y|)c] < 0$. We can also adjust h_3 to enable cavity two to interfere constructively along the x polarization direction and destructively along the y polarization direction at the same frequency. For example, we have $\tau_{\Delta\phi_2^x} = \tau_{\phi_{c2}^x} |r_{321}^x r_{34}^x| / (1 - |r_{321}^x r_{34}^x|) > 0$ and $\tau_{\Delta\phi_2^y} = -\tau_{\phi_{c2}^y} |r_{321}^y r_{34}^y| (1 + |r_{321}^y r_{34}^y|) < 0$, where $|r_{321}^x| = |(r_{21}^x - r_{23}^x)/(1 + r_{23}^x r_{21}^x)|$ and $|r_{321}^y| = |(r_{21}^y + r_{23}^y)/(1 + r_{23}^y r_{21}^y)|$ with $h_3 = Nc/2n_3 f_0$ (see Note 2 in the Supplemental Material for more details about $\tau_{\phi_{c2}^x}$ and $\tau_{\phi_{c2}^y}$ [34]). It is important to note that, in order to maximize the monotone intervals of $\Delta\phi_2^x$ and $\Delta\phi_2^y$ so that it is possible to generate a flat phase dispersion with the largest spectral bandwidth, a thinner substrate thickness is preferred for the QWP design. To briefly conclude, by appropriately choosing n_2^y, n_2^x, h_2, and h_3 to satisfy the conditions as $\phi_{c1}^y = 4\pi n_2^y h_2 f_0 / c = (2I + 1)\pi$, $\phi_{c1}^x = 4\pi n_2^x h_2 f_0 / c = 2I\pi$, and $[|r_{21}^y r_{23}^y| / (1 + |r_{21}^y r_{23}^y|)]\tau_{\phi_{c1}^y} + [|r_{21}^x r_{23}^x| / (1 - |r_{21}^x r_{23}^x|)]\tau_{\phi_{c1}^x} - \tau_{\Delta\phi_2^y} + \tau_{\Delta\phi_2^x} = 2\pi(n_2^y - n_2^x)h_2/c$, where I is an integer, the phase condition with $\phi_{\rm PD} \approx \phi'_{\rm PD} = \pi/2(\Delta\phi_1^y = \Delta\phi_1^x = 0$, $|\Delta\phi_2^y|$, $|\Delta\phi_2^x| \ll |\phi'_{PD}|$), and $\tau_{\phi_{\rm PD}} = 0$ for a broadband QWP around f_0 can be expected. It should be emphasized that there are numerous combinations of n_2^y, n_2^x, h_2, and h_3 that satisfy the phase condition for a broadband QWP. However, the minimum values of n_2^y, n_2^x, h_2, and h_3 should be used to broaden the monotone intervals of $\Delta\phi_1^x$, $\Delta\phi_1^y$, $\Delta\phi_2^x$ and $\Delta\phi_2^y$, thus maximizing the operation bandwidth for a QWP.

C. Design, fabrication, and measurement of broadband MTM QWPs

The above-mentioned concept of using MBI for phase modulation of the transmitted em waves can be used to significantly broaden the operation bandwidth of WPs based on anisotropic MTMs, which generally work within a rather narrow bandwidth due to the intrinsic phase dispersion [13,24,27,35]. Here, we choose to design and experimentally realize wideband QWPs based on a kind of anisotropic MTM that is typically comprised of an alternating metal and dielectric multilayer, which has been proposed previously for narrow-band polarization conversion [13]. It has been theoretically demonstrated that such an artificial structure can always support a branch of tailored spoof surface plasmons (SSPs) on their side walls (see Note 3 in the Supplemental Material for more details regarding the derivation process for the dispersion relation [34]). The microwave regime has been chosen to investigate the modal dispersions of the SSPs, whose dispersion relation shows strong dependence on the gap separations between the adjacent MTM units. The Cu and FR4 have the conductivity of 5×10^7 $(\Omega$ m$)^{-1}$ and the relative permittivity of $4.3 + 0.025i$, respectively, in the microwave regime [36,37].

By further using a rectangle-shaped MTM shown in Fig. 3(a), different propagation constants of the SSPs along the x and y polarization directions (k_2^x and k_2^y) are introduced [Fig. 3(b)], and thus an effective anisotropic medium can be artificially constructed. The distinct k_2^x and k_2^y can be notably reflected by the modal field distributions on the two side walls shown in Figs. 3(c) and 3(d). By using such an anisotropic medium, that is, the rectangle-shaped MTM shown in Fig. 3(a), to serve as layer two of the four-layer system, we can thus use the design approach mentioned in Sec. II B to achieve the phase conditions required for a broadband WP. Recent studies have shown that k_2^x and k_2^y are highly dependent on the geometrical parameters of the anisotropic MTM, especially the widths (W_x, W_y), the lattice constant along the z direction, P_z, and the gap separation between the adjacent MTM units ($P_x - W_x, P_y - W_y$) [37]. After carefully optimizing the geometrical parameters, we have $\phi_{c1}^x = 2\pi$ and $\phi_{c1}^y = 3\pi$ at $f_0 = 7.25$ GHz with a choice of 36-layer Cu and 35-layer FR4 [Fig. 4(a)], which enables the SSPs to interfere constructively and destructively along the x and y directions, respectively. In addition, the cross-polarization phase difference without the involvement of MBI, ϕ_{PD}', is approximately $\pi/2$ at $f_0 = 7.25$ GHz, but increases with f, which fails to construct a broadband QWP. On the basis of $\phi_{c1}^x = 2\pi$ and $\phi_{c1}^y = 3\pi$ for cavity one, it can be seen from

Fig. 4(b) that $\tau_{\Delta\phi_1^x} > 0$ and $\tau_{\Delta\phi_1^y} < 0$, which partially compensates for the phase dispersion of $\tau_{\phi'_{PD}}(> 0)$. Additional phase modulation can be imparted by cavity two, determined by the thickness of the FR4 substrate once cavity one is ready. Figure 4(c) presents the dependence of $\tau_{\Delta\phi_2^x}$ and $\tau_{\Delta\phi_2^y}$ at 7.25 GHz on the thickness of the FR4 substrate, h_3. Interestingly, it is shown that $\tau_{\Delta\phi_2^x}$ is positive and $\tau_{\Delta\phi_2^y}$ is negative as h_3 is below 4.2 mm. The phase dispersion of $\tau_{\phi'_{PD}}$ can be exactly cancelled out at around $f_0 = 7.25$ GHz [Fig. 4(b)] with a combination of cavity one and cavity two with $h_3 = 2.5$ mm. As a result, the total phase dispersion, $\tau_{\phi_{PD}}$, is equal to zero at around $f_0 = 7.25$ GHz, thanks to the MBI-enabled dispersion cancellation effects.

Choosing the designed geometrical parameters mentioned above, we successfully fabricate one sample and experimentally characterize its polarization conversion capability. In the fabrication process, each copper layer with a thickness of 0.079 mm is printed on a FR4 layer with a thickness of 0.386 mm using the method of a multilayered printed circuit board. The composite layers are sandwiched using adhesive with a thickness of 0.05 mm (almost the same dielectric constant as FR4). Thirty-six layers of copper and 35 layers of FR4 are formed by repeating the above-mentioned process. A standard mechanical milling method is then followed to shape the anisotropic MTMs, of which the top-view photograph of the fabricated
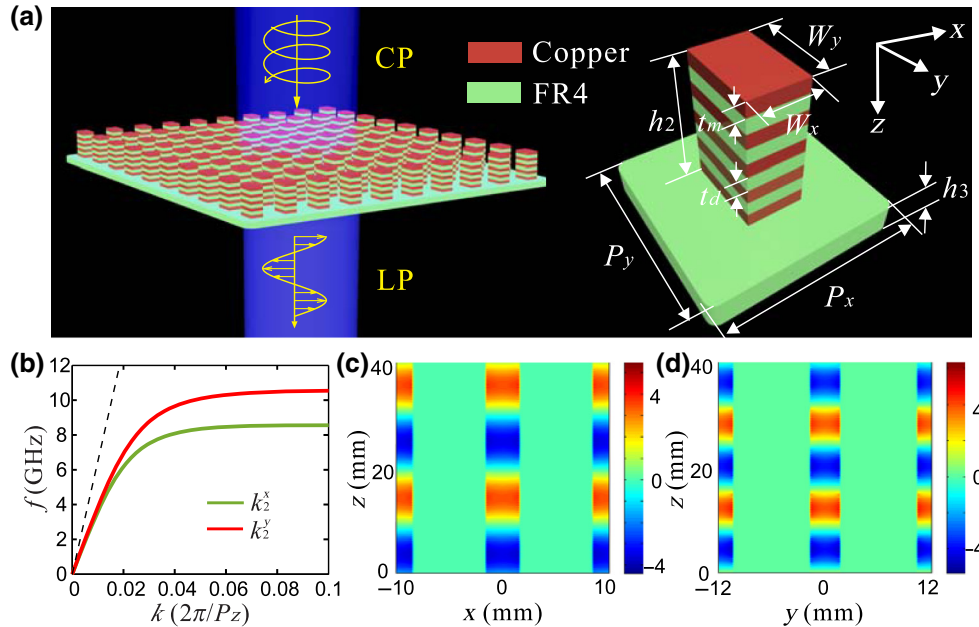

FIG. 3. (a) Schematic of a rectangle-shaped anisotropic MTM QWP, whose unit cell is illustrated on the right side. The MTM has the cross-section parameters as W_x and W_y, and the lattice constants as P_x and P_y. The thicknesses of a single layer of Cu and FR4 are represented by t_m and t_d, respectively, and the total thicknesses of the MTM and the FR4 substrate are denoted by h_2 and h_3, respectively. (b) The dispersion relations of the SSP modes for the x (green) and y (red) polarizations calculated with $W_x = 6.8$ mm, $W_y = 8.6$ mm, $P_x = 10$ mm, $P_y = 12$ mm, $t_m = 0.079$ mm, $t_d = 0.386$ mm, and $P_z = t_m + t_d = 0.465$ mm. (c),(d) The field distributions of real part of E_x in the x-z plane (c), and real part of E_y in the y-z plane (d).
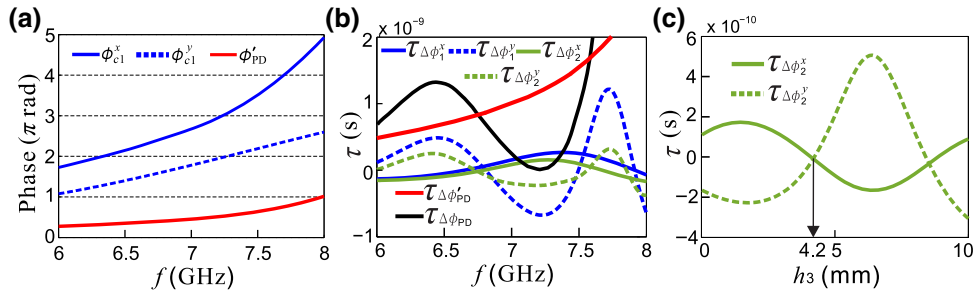
FIG. 4. (a) ϕ_{c1}^x (blue solid), ϕ_{c1}^y (blue dashed), and ϕ'_{PD} (red solid) as a function of f with 35-layer FR4 and 36-layer Cu ($h_2 = 16.35$ mm). (b) $\tau_{\Delta\phi_1^x}$ (blue solid), $\tau_{\Delta\phi_1^y}$ (blue dashed), $\tau_{\Delta\phi_2^x}$ (green solid), $\tau_{\Delta\phi_2^y}$ (green dashed), $\tau_{\phi'_{PD}}$ (red solid), and $\tau_{\phi_{PD}}$ (black solid) as a function of $\tau_{\phi_{PD}}$ with $h_3 = 2.5$ mm. (c) $\tau_{\Delta\phi_2^x}$ and $\tau_{\Delta\phi_2^y}$ as a function of h_3. The other geometrical parameters are the same as those in Fig. 3.

sample is presented in Fig. 5(a). The measurement set up is schematically shown in Fig. 5(b). It can be seen from Figs. 5(c) and 5(d) that the measured transmission amplitudes for the x and y polarizations ($|t_0^x|$ and $|t_0^y|$), the total transmission amplitude $\left(\sqrt{(|t_0^x|^2 + |t_0^y|^2)/2}\right)$, the insertion loss ($-10\log_{10}[(|t_0^x|^2 + |t_0^y|^2)/2]$), and the cross-polarization phase difference (ϕ_{PD}) are basically consistent with the simulation results. Here, we define the dispersionless band as the frequency band where the cross-polarization phase difference is within the range of $90^\circ \pm 10^\circ$. The measured dispersionless bandwidth covers the frequency range of 6.73–7.60 GHz, which is up to 12.0% of the central frequency of 7.25 GHz. Within the dispersionless band, the measured total transmission amplitude ranges from 61.5% to 73.8%, and the insertion

loss is less than 4.3 dB. The deviation of the measured and the designed device performance may result from the fabrication error and measurement imprecision. To evaluate the performance of the QWP, we use the degree of linear polarization (DoLP) to test the degree of linear polarization of the transmitted waves under the illumination of left-circularly polarized light waves from the z direction. DoLP is defined as $\mathrm{DoLP} = \sqrt{s_1^2 + s_2^2}/s_0$, where s_0, s_1, and s_2 are the Stokes parameters given by $s_0 = |E_x|^2 + |E_y|^2$, $s_1 = |E_x|^2 - |E_y|^2$, and $s_2 = E_x E_y^* + E_x^* E_y$, respectively [31]. Here, E_x^* and E_y^* denote the complex conjugates of E_x and E_y, respectively. Figure 5(d) clearly illustrates that the DoLP is kept nearly at one ($>95\%$ in the experiment) within the operation bandwidth of 6.73–7.60 GHz, indicating that the transmitted em waves are almost linearly polarized.
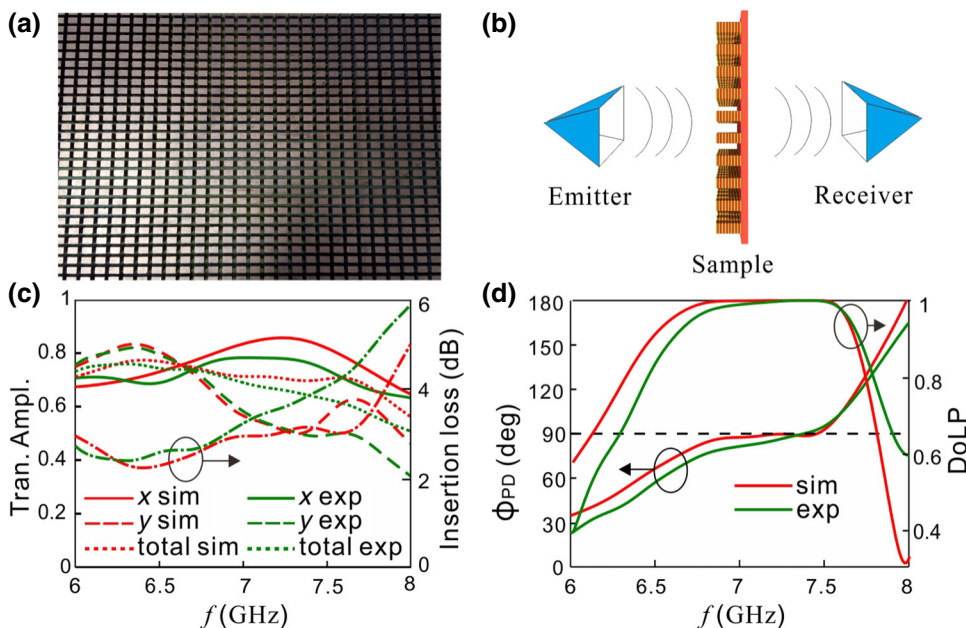

FIG. 5. (a) Photograph of the fabricated anisotropic MTM QWP sample. (b) Schematic of the experimental set up for testing the polarization conversion performance. The sample is placed between the emitter and receiver, both of which are connected to a vector network analyzer. (c) The simulated and measured transmission amplitudes for the x polarization (the solid lines) and y polarization (the dashed lines), total transmission amplitude (the dotted lines), and insertion loss (the chain lines) vs f. (d) ϕ_{PD} and DoLP as a function of f. In (c),(d), the green and red lines indicate the simulated and experimental results, respectively.

D. Extension to high frequencies

The key factor to design a WP based on MBI in any spectral regime lies in finding an artificial anisotropic structure that experiences different propagation constants along the x and y directions. Previous studies have proven the giant birefringence with the anisotropic MTMs, that is, a rectangle-shaped metal and dielectric multilayer [13,37, 38]. Further, we can introduce zero phase dispersion by carefully designing the geometrical parameters to make the MTM work under constructive and destructive interferences for the x and y polarizations, respectively. Since the design strategy mentioned above is so general, one can employ it to address the issue of narrow bandwidth in higher-frequency domains.

Here, as a demonstration, we extend the operation bandwidth of the QWP based on anisotropic MTMs to telecom and terahertz frequencies. The anisotropic MTM at telecom frequencies composes an Ag/SiO$_2$ multilayer [Fig. 6(a)], with the thicknesses of each SiO$_2$ and Ag layer being $t_d = 35$ nm and $t_m = 35$ nm, respectively [39]. Eight pairs of Ag/SiO$_2$ layers are adopted, resulting in a total thickness of 560 nm for the anisotropic MTM. The cross-section dimensions of the anisotropic MTM are set as $Wx = 223$ nm and $Wy = 240$ nm, and the lattice constants along the x and y axes are $Px = Py = 280$ nm. Considering the practical applications, it is assumed that the anisotropic MTM (serves as layer two) is deposited on a semi-infinite SiO$_2$ substrate, resulting in a three-layer system. In this case, the total transmission coefficient is t_{123}, as given by Eq. (1). The cross-polarization phase difference for the three-layer system can be expressed as

$$\phi_{PD} = \arg t^y_{123} - \arg t^x_{123} = \phi'_{PD} + \Delta\phi^y_1 - \Delta\phi^x_1. \quad (9)$$

We only need to take into account the phase modulation from cavity one, but neglect the influence of cavity two on the phase dispersion of the transmitted em waves. With the carefully designed structural parameters of the anisotropic MTMs, constructive or destructive interference is imparted on the x and y polarizations at around 193.5 THz (1550 nm). This can be reflected by the cross-polarization transmission amplitudes shown in Fig. 6(b), where $|t^x_{123}|$ and $|t^y_{123}|$ reach the maximum and minimum values, respectively, at around 1550 nm. The simulated results shown in Fig. 6(c) verify that the designed QWP can keep the cross-polarization phase difference within the range of $90° \pm 10°$ over a wide wavelength band of 1503–1716 nm (the dispersionless band), 13.6% with respect to 1550 nm. Within the dispersionless band of 1503–1716 nm, the total transmission amplitude $\left(\sqrt{(|t^x_{123}|^2 + |t^y_{123}|^2)/2} \right)$ reaches about 72%, associated with the insertion loss ($-10\log_{10}[n_3(|t^x_{123}|^2 + |t^y_{123}|^2)/2]$) of less than 1.3 dB [Fig. 6(b)], and the DoLP is above 98% [Fig. 6(c)].
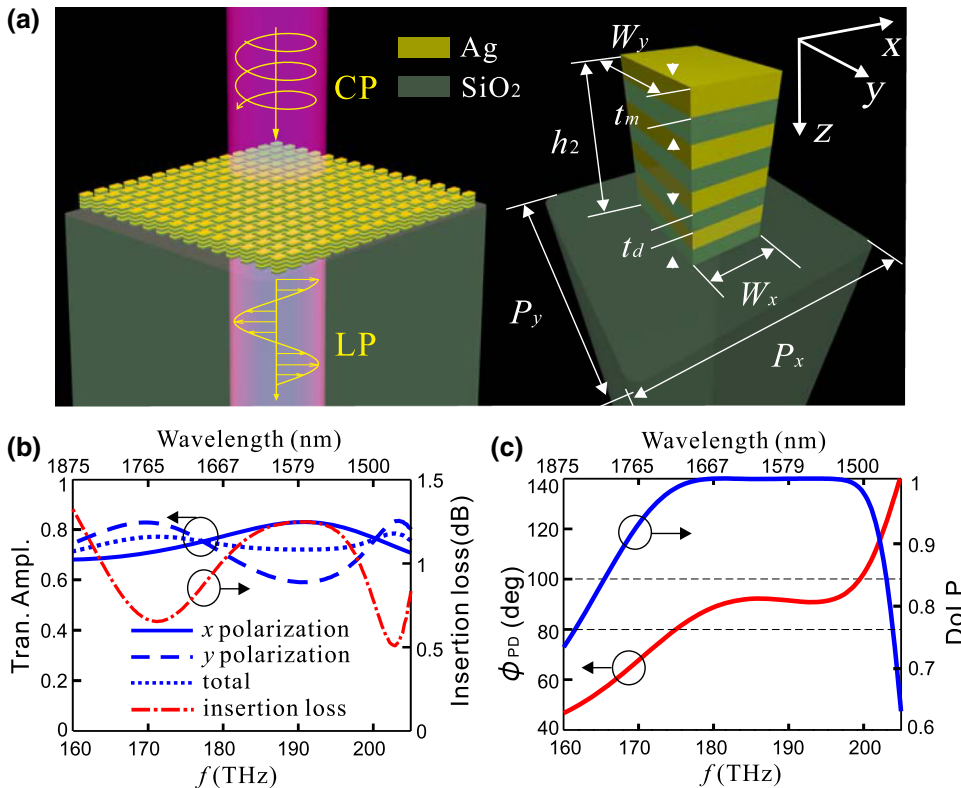

FIG. 6. (a) Schematic of the anisotropic MTM QWP at telecom wavelength, with the geometric parameters for a unit cell being shown on the right side. (b) Transmission amplitudes for the x and y polarizations, total transmission amplitude, and insertion loss vs f. (c) ϕ_{PD} (red) and DoLP (blue) as a function of f. The two horizontal dashed lines in (c) correspond to 80° and 100°.

Following the design approach for the telecom frequencies, we design a broadband MTM QWP based on an Al/GaAs multilayer in the terahertz regime. The designed one can keep the ϕ_{PD} within the range of $90^o \pm 10°$ over a wide frequency range of 1.51–2.19 THz (the dispersionless band), 35.8% with respect to the central frequency of 1.9 THz. The total transmission amplitude reaches up to approximately 65%, associated with the insertion loss of less than 2.4 dB, and the DoLP is above 98% in the dispersionless band. For more details regarding the performance of the device, please see Note 4 in the Supplemental Material [34].

To experimentally implement the proposal at infrared and terahertz frequencies, we can first use deposition techniques, such as magnetron sputtering system or electron beam evaporation, to precisely grow the metal and dielectric multilayer. The final anisotropic MTMs are achievable with mature etching techniques such as focused ion-beam milling and reactive ion etching.

III. CONCLUSION

In summary, we show that a classical MBI mechanism can be employed to modulate the phase dispersion of transmitted em waves in MTMs, where an additional positive or negative phase shift is caused by constructive or destructive interference. Based on the MBI-enabled phase dispersion modulation mechanism, a general strategy is established to achieve a dispersionless cross-polarization phase difference by independently controlling the interference condition for the two orthogonal polarization directions. We design a broadband anisotropic MTM QWP and experimentally verify that it can realize circular-linear polarization conversion with a total transmission amplitude ranging from 61.5% to 73.8% within the dispersionless bandwidth of 6.73–7.60 GHz. This design strategy can also be extended to optical frequencies, and we employ full-wave simulations to demonstrate broadband QWPs at telecom and terahertz frequencies. The proposed anisotropic MTM WPs show superiority over the previous proposals in transmission mode, which typically rely on decoupled resonance to achieve a cross-polarization phase difference, and hence have limited operation bandwidth near the resonance frequency [24, 26]. Our findings can stimulate designing dispersion-controlled high-performance wave manipulation components in microwave, terahertz, and optical regimes.

ACKNOWLEDGMENTS

[1] H. Kikuta, Y. Ohira, and K. Iwata, Achromatic quarter-wave plates using the dispersion of form birefringence, Appl. Opt. **36**, 1566 (1997).

[2] W. Yu, A. Mizutani, H. Kikuta, and T. Konishi, Reduced wavelength-dependent quarter-wave plate fabricated by a multilayered subwavelength structure, Appl. Opt. **45**, 2601 (2006).

[3] D. Schurig, J. Mock, B. Justice, S. A. Cummer, J. B. Pendry, A. Starr, and D. Smith, Metamaterial electromagnetic cloak at microwave frequencies, Science **314**, 977 (2006).

[4] N. I. Landy, S. Sajuyigbe, J. Mock, D. Smith, and W. Padilla, Perfect Metamaterial Absorber, Phys. Rev. Lett. **100**, 207402 (2008).

[5] H.-T. Chen, W. J. Padilla, M. J. Cich, A. K. Azad, R. D. Averitt, and A. J. Taylor, A metamaterial solid-state terahertz phase modulator, Nat. Photonics **3,** 148 (2009).

[6] J. K. Gansel, M. Thiel, M. S. Rill, M. Decker, K. Bade, V. Saile, G. von Freymann, S. Linden, and M. Wegener, Gold helix photonic metamaterial as broadband circular polarizer, Science **325**, 1513 (2009).

[7] D. Lin, P. Fan, E. Hasman, and M. L. Brongersma, Dielectric gradient metasurface optical elements, Science **345,** 298 (2014).

[8] Y. Xiang, X. Dai, J. Guo, H. Zhang, S. Wen, and D. Tang, Critical coupling with graphene-based hyperbolic metamaterials, Sci. Rep. **4**, 5483 (2014).

[9] T. Lv, Y. Li, H. Ma, Z. Zhu, Z. Li, C. Guan, J. Shi, H. Zhang, and T. Cui, Hybrid metamaterial switching for manipulating chirality based on VO$_2$ phase transition, Sci. Rep. **6**, 23186 (2016).

[10] J. Shi, Z. Li, D. K. Sang, Y. Xiang, J. Li, S. Zhang, and H. Zhang, THz photonics in two dimensional materials and metamaterials: Properties, devices and prospects, J Mater. Chem. C **6**, 1291 (2018).

[11] J. Hao, Y. Yuan, L. Ran, T. Jiang, J. A. Kong, C. T. Chan, and L. Zhou, Manipulating Electromagnetic Wave Polarizations by Anisotropic Metamaterials, Phys. Rev. Lett. **99,** 063908 (2007).

[12] Y. Dai, H. Cai, H. Ding, Z. Ning, N. Pan, H. Zhu, Q. Shi, and X. Wang, Near-infrared quarter-waveplate with near-unity polarization conversion efficiency based on silicon nanowire array, Opt. Express **23**, 8929 (2015).

[13] H. Zhu, X. Yin, L. Chen, Z. Zhu, and X. Li, Manipulating light polarizations with a hyperbolic metamaterial waveguide, Opt. Lett. **40**, 4595 (2015).

[14] M. Chen, F. Fan, S. Xu, and S. Chang, Artificial high birefringence in all-dielectric gradient grating for broadband terahertz waves, Sci. Rep. **6**, 38562 (2016).

[15] X. Ma, W. Pan, C. Huang, M. Pu, Y. Wang, B. Zhao, J. Cui, C. Wang, and X. Luo, An active metamaterial for polarization manipulating, Adv. Opt. Mater. **2**, 945 (2014).

[16] Y. Li, J. Zhang, S. Qu, H. Ma, J. Wang, J. Wang, and Z. Xu, High-efficiency polarization conversion based on spatial

dispersion modulation of spoof surface plasmon polaritons, Opt. Express **24**, 24938 (2016).

[17] A. Pors, M. G. Nielsen, and S. I. Bozhevolnyi, Broadband plasmonic half-wave plates in reflection, Opt. Lett. **38**, 513 (2013).

[18] F. Ding, Z. Wang, S. He, V. M. Shalaev, and A. V. Kildishev, Broadband high-efficiency half-wave plate: a supercell-based plasmonic metasurface approach, ACS Nano **9**, 4111 (2015).

[19] S. Jiang, X. Xiong, Y. Hu, Y. Hu, G. Ma, R. Peng, C. Sun, and M. Wang, Controlling the Polarization State of Light with a Dispersion-Free Metastructure, Phys. Rev. X **4**, 021026 (2014).

[20] J. Kim, S. Choudhury, C. DeVault, Y. Zhao, A. V. Kildishev, V. M. Shalaev, A. Alù, and A. Boltasseva, Controlling the polarization state of light with plasmonic metal oxide metasurface, ACS Nano **10**, 9326 (2016).

[21] H. Ma, G. Wang, G. Kong, and T. Cui, Broadband circular and linear polarization conversions realized by thin birefringent reflective metasurfaces, Opt. Mater. Express **4**, 1717 (2014).

[22] W. Liu, S. Chen, Z. Li, H. Cheng, P. Yu, J. Li, and J. Tian, Realization of broadband cross-polarization conversion in transmission mode in the terahertz region using a single-layer metasurface, Opt. Lett. **40**, 3185 (2015).

[23] A. C. Strikwerda, K. Fan, H. Tao, D. V. Pilon, X. Zhang, and R. D. Averitt, Comparison of birefringent electric split-ring resonator and meanderline structures as quarter-wave plates at terahertz frequencies, Opt. Express **17**, 136 (2009).

[24] Y. Zhao and A. Alù, Manipulating light polarization with ultrathin plasmonic metasurfaces, Phys. Rev. B **84**, 205428 (2011).

[25] Z. Li, W. Liu, H. Cheng, S. Chen, and J. Tian, Realizing broadband and invertible linear-to-circular polarization converter with ultrathin single-layer metasurface, Sci. Rep. **5**, 18106 (2015).

[26] W. Sun, Q. He, J. Hao, and L. Zhou, A transparent metamaterial to manipulate electromagnetic wave polarizations, Opt. Lett. **36**, 927 (2011).

[27] Y. Zhao and A. Alù, Tailoring the dispersion of plasmonic nanorods to realize broadband optical meta-waveplates, Nano Lett. **13**, 1086 (2013).

[28] C. Huang, Efficient and broadband polarization conversion with the coupled metasurfaces, Opt. Express **23**, 32015 (2015).

[29] Y. Zhang, Y. Feng, B. Zhu, J. Zhao, and T. Jiang, Switchable quarter-wave plate with graphene based metamaterial for broadband terahertz wave manipulation, Opt. Express **23**, 27230 (2015).

[30] L. Cong, N. Xu, J. Gu, R. Singh, J. Han, and W. Zhang, Highly flexible broadband terahertz metamaterial quarter-wave plate, Laser Photon. Rev. **8**, 626 (2014).

[31] X. Ke, H. Zhu, J. Li, L. Chen, and X. Li, Double-stacked hyperbolic metamaterial waveguide arrays for efficient and broadband terahertz quarter-wave plates, Sci. Rep. **7**, 574 (2017).

[32] L. Zhou, H. Li, Y. Qin, Z. Wei, and C. Chan, Directive emissions from subwavelength metamaterial-based cavities, Appl. Phys. Lett. **86**, 101101 (2005).

[33] H. Chen, J. Zhou, J. F. O'Hara, F. Chen, A. K. Azad, and A. J. Taylor, Antireflection Coating using Metamaterials and Identification of its Mechanism, Phys. Rev. Lett. **105**, 073901 (2010).

[34] See the Supplemental Material at http://link.aps.org/supplemental/10.1103/PhysRevApplied.11.044042 for derivation process of Eqs. (5) and (6) (Note 1), derivation process of $\tau_{\phi_{c2}^x}$ and $\tau_{\phi_{c2}^y}$ (Note 2), theoretical calculation of the dispersion relation of the SSP mode supported by a one-dimensional anisotropic MTM composed of metal and dielectric multilayer (Note 3), and the broadband QWP in the terahertz regime (Note 4).

[35] Z. Jiang, L. Lin, D. Ma, S. Yun, D. Werner, Z. Liu, and T. S. Mayer, Broadband and wide field-of-view plasmonic metasurface-enabled waveplates, Sci. Rep. **4**, 7511 (2014).

[36] X. Yin, C. Long, J. Li, H. Zhu, L. Chen, J. Guan, and X. Li, Ultra-wideband microwave absorber by connecting multiple absorption bands of two different-sized hyperbolic metamaterial waveguide arrays, Sci. Rep. **5**, 15367 (2015).

[37] X. Yin, H. Zhu, H. Guo, M. Deng, T. Xu, Z. Gong, X. Li, Z. Hang, C. Wu, H. Li, S. Chen, L. Zhou, and L. Chen, Hyperbolic metamaterial devices for wavefront manipulation, Laser Photon. Rev. **13**, 1800081 (2019).

[38] A. Poddubny, I. Iorsh, P. Belov, and Y. Kivshar, Hyperbolic metamaterials, Nat. Photonics **7**, 948 (2013).

[39] E. Palik, *Handbook of Optical Constants of Solids II* (Academic, New York, 1991).